



FORMULATION OF THE TIME-VARYING FUNCTION OF MOMENTARY ENERGY INPUT TO A SINGLE-DEGREE-OF-FREEDOM SYSTEM USING FOURIER SERIES

Kenji FUJII¹, Hideto KANNO² and Tetsuya NISHIDA³

¹ Member, Professor, Dept. of Architecture, Chiba Institute of Technology,
Narashino, Chiba, Japan, kenji.fujii@it-chiba.ac.jp

² Member, Professor, Dept. of Architecture and Environment System, Akita Prefectural University,
Yuri-Honjyo, Akita, Japan, kanno@akita-pu.ac.jp

³ Member, Professor, Dept. of Architecture and Environment System, Akita Prefectural University,
Yuri-Honjyo, Akita, Japan, tetsuya_nishida@akita-pu.ac.jp

ABSTRACT: This article derives a time-varying function of the momentary energy input to a linear elastic single-degree-of-freedom system with viscous and complex damping. The problem is formulated in the form of a Fourier series using the Fourier amplitude and the difference of Fourier phase angles. The numerical analysis results show that (1) the time-varying function formulated using the Fourier series corresponds to the envelope of ground acceleration, and (2) the maximum momentary input energy evaluated using the formulation in this paper agrees well with that obtained from time-history analysis.

Keywords: Fourier series, Time-varying function, Momentary energy input

1. INTRODUCTION

In the seismic design of building structures, the most important response parameter is the peak displacement. Another important parameter is the cumulative energy absorbed by the structure. The *total input energy*^{1), 2)} is the seismic intensity parameter related to the cumulative energy. Moreover, the *maximum momentary input energy*³⁾⁻⁵⁾ is the intensity parameter related to the peak displacement.

The total input energy is the energy input to a structure from the beginning to the end of the earthquake excitation. Kuwamura et al.⁶⁾ and Ordaz⁷⁾ have shown that the total input energy per unit mass can be calculated from a Fourier amplitude spectrum without the phase characteristics of ground acceleration. Additionally, the momentary input energy strongly depends on the energy input per unit time. Ohsaki revealed that the waveform of the ground acceleration is strongly correlated with the distribution of its phase difference⁸⁾, so the time history of the momentary energy input should be related to the phase characteristics of ground acceleration. Kuwamura⁹⁾ and Takahashi and Akiyama¹⁰⁾ demonstrated that the time history of the cumulative energy input is similar to that of the cumulative square of the acceleration. However, the relation between the phase characteristics of ground motion and its cumulative square remains unknown.

The authors have investigated the relation between the total input energy¹⁾, E_I , and the maximum momentary input energy^{3),4)}, ΔE_{\max} , from the viewpoint of the duration of ground acceleration¹¹⁾. In a previous study¹¹⁾, the equivalent duration of ground acceleration was defined from the distribution of the group delay time¹²⁾. The relation between E_I and ΔE_{\max} was then formulated as a function of the equivalent duration. However, the definition of equivalent duration in this previous study was not supported by a theoretical background. Therefore, there is still room for further discussion on this point.

The authors have also developed a method that predicts the peak response of pre-1981-designed existing reinforced concrete (RC) and steel reinforced concrete (SRC) structures with brittle members. During a series of analytical¹³⁾⁻¹⁵⁾ and experimental^{16),17)} studies, it was found that the peak displacement of existing concrete structures with brittle members depends strongly on the time history of ground acceleration, even though its response spectrum is the same¹³⁾.

It is important to note that the time-history of the acceleration is *not* uniquely determined from the Fourier amplitude and Fourier phase difference. Kimura has shown that a new ground acceleration can be generated artificially from the original acceleration by shifting the Fourier phase angle¹⁸⁾: the waveform of the generated acceleration is similar to that of the original acceleration, but its time-history is locally different. Analytical studies have investigated the nonlinear response of a seven-story SRC existing building^{14), 15)} using groups of ground accelerations; in these analyses, the same target response spectrum and Fourier phase difference were used to generate the ground accelerations. The only difference in the group of generated ground accelerations was the value of the shifted phase angle. The results show that nonnegligible scattering of the peak displacement occurs, even though the response spectrum and Fourier phase difference of the input ground motions are identical¹⁴⁾. In addition, the peak response of structures with brittle members strongly depends on whether significant strength degradation occurs prior to the maximum momentary energy input¹⁵⁾. Note that scattering of the nonlinear peak response due to local differences in the input ground motion is observed in the response of an SRC building without brittle members¹⁹⁾.

As discussed in previous studies^{13), 15)}, premature brittle failure prior to the maximum momentary energy input strongly depends on the cumulative energy input until the maximum momentary energy input. Therefore, for better predictions of the peak displacement of a building with brittle members, accurate predictions of (i) the maximum momentary input energy and (ii) the cumulative input energy until the maximum momentary energy input are essential. As stated above, the time-history of the acceleration is *not* uniquely determined from the Fourier amplitude and Fourier phase difference. The authors consider the scattering of the nonlinear response caused by local differences in ground acceleration to be unavoidable “fluctuations.” Therefore, the influence of such unavoidable fluctuations should be eliminated from the prediction method for both (i) and (ii).

In this article, a time-varying function of the momentary energy input to a linear elastic single-degree-of-freedom (SDOF) system is formulated. Section 2 derives the time-varying function of ground acceleration in the form of a Fourier series. Section 3 describes the formulation of a time-varying function of the momentary energy input to a linear elastic SDOF system with viscous and complex damping. Section 4 presents numerical examples and validates the proposed time-varying function, before verifying the accuracy of the predicted maximum momentary input energy based on the proposed time-varying function.

2. TIME-VARYING FUNCTION OF GROUND ACCELERATION

2.1 Definition of the time-varying function and envelope function of ground acceleration

A discrete time history of ground motions $a_g(t)$, defined within the range $[0, t_d]$, can be expressed as follows using a Fourier series:

$$a_g(t) = \sum_{n=-N}^N c_n \exp(i\omega_n t), \quad (1)$$

$$\omega_n = n\Delta\omega = n \cdot (2\pi/t_d), \omega_{-n} = -\omega_n = -n\Delta\omega, \quad (2)$$

$$c_n = \frac{1}{t_d} \int_0^{t_d} a_g(t) \exp(-i\omega_n t) dt, c_{-n} = \frac{1}{t_d} \int_0^{t_d} a_g(t) \exp(i\omega_n t) dt = \overline{c_n}. \quad (3)$$

In Eqs. (1)–(3), c_n and ω_n are the complex Fourier coefficients of the ground motion and the circular frequency of the n^{th} harmonic, and i is the imaginary unit. Additionally, it is assumed that c_0 is equal to zero. In Eq. (3), the overbar indicates the complex conjugate. Let A_n and ϕ_n be the Fourier amplitude and phase angle of the n^{th} harmonic. The relation between A_n , ϕ_n , c_n , and $\overline{c_n}$ is

$$|c_n| = |c_{-n}| = A_n/2, c_n = (A_n/2) \exp(-i\phi_n), c_{-n} = \overline{c_n} = (A_n/2) \exp(i\phi_n). \quad (4)$$

Following a study by Kimura¹⁸⁾, the ground motion $a_g^*(t)$ can be defined from Eq. (1) by shifting the phase angle of all harmonics by $\pi/2$, i.e.,

$$a_g^*(t) = \sum_{n=-N}^N c_n \exp\left[i\left\{\omega_n t - \text{sgn}(\omega_n) \frac{\pi}{2}\right\}\right] = -i \sum_{n=-N}^N c_n \text{sgn}(\omega_n) \exp(i\omega_n t), \quad (5)$$

$$\text{sgn}(\omega_n) = \begin{cases} 1 & \omega_n > 0 \\ -1 & \omega_n < 0 \end{cases}. \quad (6)$$

Note that the ground acceleration given by Eq. (5) corresponds to the Hilbert transform of the original ground acceleration in Eq. (1). The time-varying function and the envelope function of the ground acceleration, $\widehat{a}_g(t)$ and $\alpha(t)$, respectively, are defined as

$$\widehat{a}_g(t) = \sqrt{\left[\{a_g(t)\}^2 + \{a_g^*(t)\}^2\right] / 2}, \quad (7)$$

$$\alpha(t) = \sqrt{2} \widehat{a}_g(t) = \sqrt{\{a_g(t)\}^2 + \{a_g^*(t)\}^2}. \quad (8)$$

Figure 1 compares the ground acceleration motions $a_g(t)$, $a_g^*(t)$ and the envelope function $\alpha(t)$. The ground acceleration used herein is the horizontal major component of the Osaka Gas Fukiai record from the 1995 Hyogo-ken Nanbu Earthquake. As shown here, although the time-history of the original record $a_g(t)$ and its Hilbert transform $a_g^*(t)$ are different, the waveforms of these two accelerations are similar. In addition, the function $\alpha(t)$ envelops both $a_g(t)$ and $a_g^*(t)$.

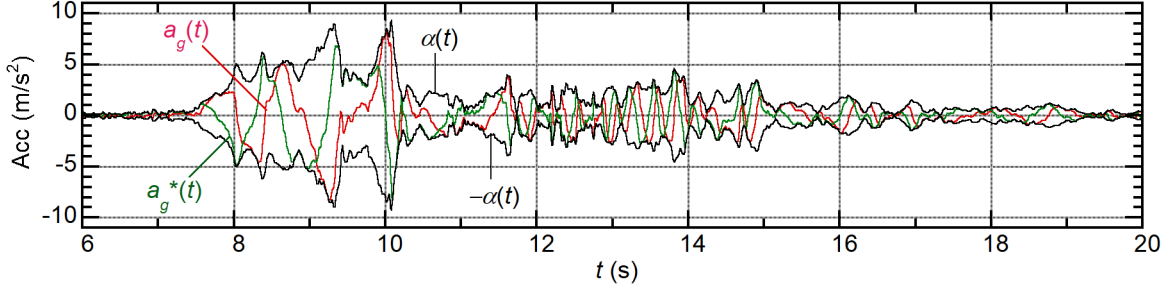


Fig. 1 Comparison of $a_g(t)$, $a_g^*(t)$ and envelope function $\alpha(t)$

2.2 Formulation of the time-varying function using Fourier series

Substituting Eqs. (1) and (5) into Eq. (7), the time-varying function $\widehat{a}_g(t)$ can be rewritten as

$$\widehat{a}_g(t) = \frac{1}{\sqrt{2}} \left[\left\{ \sum_{n=-N}^N c_n \exp(i\omega_n t) \right\}^2 - \left\{ \sum_{n=-N}^N c_n \operatorname{sgn}(\omega_n) \exp(i\omega_n t) \right\}^2 \right]^{1/2}. \quad (9)$$

Equation (9) can be rewritten in the form

$$\{\widehat{a}_g(t)\}^2 = 2 \left\{ \sum_{n=1}^N c_n \exp(i\omega_n t) \right\} \left\{ \sum_{n=1}^N c_{-n} \exp(-i\omega_n t) \right\}. \quad (10)$$

From Eq. (10), the square of the time-varying function of ground acceleration can be expressed in the form of a Fourier series as

$$\{\widehat{a}_g(t)\}^2 = \sum_{n=-N+1}^{N-1} {}_2A_{G,n}^* \exp(i\omega_n t), \quad (11)$$

$$\text{where } {}_2A_{G,n}^* = \begin{cases} 2 \sum_{n_1=n+1}^N c_{n_1} c_{-(n_1-n)} & : n \geq 0 \\ {}_2A_{G,-n}^* & : n < 0 \end{cases}. \quad (12)$$

Equations (11) and (12) are derived in Appendix A. The envelope function $\alpha(t)$ can be calculated from

$$\alpha(t) = \sqrt{2} \widehat{a}_g(t) = \sqrt{2 \sum_{n=-N+1}^{N-1} {}_2A_{G,n}^* \exp(i\omega_n t)}. \quad (13)$$

2.3 Characteristics of the time-varying function

The average of Eq. (11) in the range $[0, t_d]$ can be expressed as

$$\left\langle \{\widehat{a}_g(t)\}^2 \right\rangle = \frac{1}{t_d} \int_0^{t_d} \sum_{n=-N+1}^{N-1} {}_2A_{G,n}^* \exp(i\omega_n t) dt = {}_2A_{G,0}^* = 2 \sum_{n_1=1}^N |c_{n_1}|^2. \quad (14)$$

In addition, the square mean value of Eqs. (1) and (5) can be expressed as

$$\left\langle \{a_g(t)\}^2 \right\rangle = \frac{1}{t_d} \int_0^{t_d} \left\{ \sum_{n=-N}^N c_n \exp(i\omega_n t) \right\}^2 dt = 2 \sum_{n=1}^N |c_n|^2 = \left\langle \{a_g^*(t)\}^2 \right\rangle. \quad (15)$$

Therefore, the square mean value of the time-varying function $\widehat{a}_g(t)$ is equal to that of the original ground acceleration and its Hilbert transform. In other words, the cumulative power of $\widehat{a}_g(t)$ is equal to that of the original acceleration $a_g(t)$.

Next, the coefficient ${}_2A_{G,n}^*$ is rewritten using the Fourier amplitude and the phase angle. In the case of $1 \leq n \leq N-1$, the coefficient ${}_2A_{G,n}^*$ can be rewritten as

$${}_2A_{G,n}^* = 2 \sum_{n_1=n+1}^N c_{n_1} c_{-(n_1-n)} = \frac{1}{2} \sum_{n_1=n+1}^N A_{n_1} A_{n_1-n} \exp\{-i(\phi_{n_1} - \phi_{n_1-n})\}. \quad (16)$$

The n^{th} phase difference, $\Delta\phi_n$, is defined as

$$\Delta\phi_n = \phi_{n+1} - \phi_n. \quad (17)$$

The difference between the phase angles in Eq. (16) can be rewritten as

$$\phi_{n_1} - \phi_{n_1-n} = \sum_{n_2=0}^{n-1} (\phi_{n_1-n_2} - \phi_{n_1-n_2-1}) = \sum_{n_2=0}^{n-1} \Delta\phi_{n_1-n_2-1}. \quad (18)$$

By substituting Eq. (18) into Eq. (16), the coefficient ${}_2A_{G,n}^*$ can be rewritten as

$${}_2A_{G,n}^* = 2 \sum_{n_1=n+1}^N c_{n_1} c_{-(n_1-n)} = \frac{1}{2} \sum_{n_1=n+1}^N A_{n_1} A_{n_1-n} \exp\left(-i \sum_{n_2=0}^{n-1} \Delta\phi_{n_1-n_2-1}\right). \quad (19)$$

As the coefficient ${}_2A_{G,-n}^*$ is the complex conjugate of ${}_2A_{G,n}^*$, ${}_2A_{G,-n}^*$ can be expressed as

$${}_2A_{G,-n}^* = \overline{{}_2A_{G,n}^*} = \frac{1}{2} \sum_{n_1=n+1}^N A_{n_1} A_{n_1-n} \exp\left(i \sum_{n_2=0}^{n-1} \Delta\phi_{n_1-n_2-1}\right). \quad (20)$$

Equations (19) and (20) indicate that the coefficients ${}_2A_{G,n}^*$, ${}_2A_{G,-n}^*$ are functions of the k^{th} Fourier amplitude A_k and the k^{th} phase difference $\Delta\phi_k$. Therefore, the time-varying function of the ground acceleration *phase-shifted* by the constant $\Delta\phi_0$, $a_g(\Delta\phi_0, t)$, is identical to that of the original ground acceleration:

$$a_g(\Delta\phi_0, t) = \sum_{n=-N}^N c_n \exp[i\{\omega_n t - \text{sgn}(\omega_n) \Delta\phi_0\}] \quad (21)$$

3. TIME-VARYING FUNCTION OF MOMENTARY INPUT ENERGY

3.1 Linear SDOF system with viscous and complex damping

In general, a linear SDOF system with either viscous or complex damping is considered. This study examines a linear SDOF system with viscous *and* complex damping, because this enables the cumulative viscous damping energy and hysteresis energy of the nonlinear system to be evaluated separately.

Considering the steady response of the linear SDOF system with viscous and complex damping under harmonic excitation (circular frequency of excitation: ω_n), the equation of motion is

$$\ddot{y} + 2h\omega_0\dot{y} + \{1 + 2\beta i \operatorname{sgn}(\omega_n)\}\omega_0^2 y = \exp(i\omega_n t). \quad (22)$$

where h and β are the viscous and complex damping ratios, respectively; ω_n is the natural circular frequency of the linear SDOF system. The response displacement and velocity of the system are

$$y(t) = H_{CVD}(i\omega_n) \exp(i\omega_n t), \dot{y}(t) = H_{CVV}(i\omega_n) \exp(i\omega_n t), \quad (23)$$

$$H_{CVD}(i\omega_n) = \frac{1}{\omega_0^2 - \omega_n^2 + 2\omega_0\{h\omega_n + \beta\omega_0 \operatorname{sgn}(\omega_n)\}i}, H_{CVV}(i\omega_n) = i\omega_n H_{CVD}(i\omega_n). \quad (24)$$

In Eqs. (23) and (24), $H_{CVD}(i\omega_n)$ and $H_{CVV}(i\omega_n)$ are the displacement and velocity transfer functions, respectively. Next, we formulate the steady response of the linear SDOF system subjected to the ground acceleration $a_g(t)$ defined in Eq. (1). The equation of motion, and the displacement and velocity responses, are expressed as

$$\ddot{y} + 2h\omega_0\dot{y} + \{1 + 2\beta i \operatorname{sgn}(\omega)\}\omega_0^2 y = -a_g(t) = -\left\{ \sum_{n=-N}^N c_n \exp(i\omega_n t) \right\}, \quad (25)$$

$$y(t) = -\sum_{n=-N}^N c_n H_{CVD}(i\omega_n) \exp(i\omega_n t), \quad (26)$$

$$\dot{y}(t) = -\sum_{n=-N}^N c_n H_{CVV}(i\omega_n) \exp(i\omega_n t). \quad (27)$$

Similarly, the equation of motion and the displacement and velocity responses of the linear SDOF system subjected to ground acceleration $a_g^*(t)$ defined in Eq. (5) are expressed as

$$\ddot{y}^* + 2h\omega_0\dot{y}^* + \{1 + 2\beta i \operatorname{sgn}(\omega)\}\omega_0^2 y^* = -a_g^*(t) = -i \left\{ \sum_{n=-N}^N c_n \operatorname{sgn}(\omega_n) \exp(i\omega_n t) \right\}, \quad (28)$$

$$y^*(t) = -i \sum_{n=1}^N c_n \operatorname{sgn}(\omega_n) H_{CVD}(i\omega_n) \exp(i\omega_n t), \quad (29)$$

$$\dot{y}^*(t) = -i \sum_{n=1}^N c_n \operatorname{sgn}(\omega_n) H_{CVV}(i\omega_n) \exp(i\omega_n t). \quad (30)$$

3.2 Time-varying function of displacement and velocity responses

The time-varying functions of the displacement and velocity responses, $\hat{y}(t)$ and $\hat{\dot{y}}(t)$, respectively, are defined as

$$\hat{y}(t) = \sqrt{\left[\{y(t)\}^2 + \{y^*(t)\}^2 \right] / 2}, \quad (31)$$

$$\hat{\dot{y}}(t) = \sqrt{\left[\{\dot{y}(t)\}^2 + \{\dot{y}^*(t)\}^2 \right] / 2}. \quad (32)$$

These can be expressed in the form of Fourier series as

$$\left\{ \hat{y}(t) \right\}^2 = \sum_{n=-N+1}^{N-1} {}_2Y_n^* \exp(i\omega_n t), \quad (33)$$

$$\text{where } {}_2Y_n^* = \begin{cases} 2 \sum_{n_1=n+1}^N H_{CVD}(i\omega_{n_1}) H_{CVD}(-i\omega_{n_1-n}) c_{n_1} c_{-(n_1-n)} & : n \geq 0 \\ \overline{{}_2Y_{-n}^*} & : n < 0 \end{cases}. \quad (34)$$

$$\left\{ \hat{\dot{y}}(t) \right\}^2 = \sum_{n=-N+1}^{N-1} {}_2V_n^* \exp(i\omega_n t), \quad (35)$$

$$\text{where } {}_2V_n^* = \begin{cases} 2 \sum_{n_1=n+1}^N H_{CVR}(i\omega_{n_1}) H_{CVR}(-i\omega_{n_1-n}) c_{n_1} c_{-(n_1-n)} & : n \geq 0 \\ \overline{{}_2V_{-n}^*} & : n < 0 \end{cases}. \quad (36)$$

The square mean value of the time-varying function of the displacement response is

$$\left\langle \left\{ \hat{y}(t) \right\}^2 \right\rangle = \frac{1}{t_d} \int_0^{t_d} \sum_{n=-N+1}^{N-1} {}_2Y_n^* \exp(i\omega_n t) dt = {}_2Y_0^* = 2 \sum_{n_1=1}^N \left| H_{CVD}(i\omega_{n_1}) \right|^2 |c_{n_1}|^2. \quad (37)$$

Similarly, the square mean value of the time-varying function of the velocity response is

$$\left\langle \left\{ \hat{\dot{y}}(t) \right\}^2 \right\rangle = \frac{1}{t_d} \int_0^{t_d} \sum_{n=-N+1}^{N-1} {}_2V_n^* \exp(i\omega_n t) dt = {}_2V_0^* = 2 \sum_{n_1=1}^N \left| H_{CVR}(i\omega_{n_1}) \right|^2 |c_{n_1}|^2. \quad (38)$$

Following the work of Sagami et al.²⁰⁾, the response period, T' , is defined as

$$T' = 2\pi \sqrt{\left\langle \left\{ \hat{y}(t) \right\}^2 \right\rangle / \left\langle \left\{ \hat{\dot{y}}(t) \right\}^2 \right\rangle} = 2\pi \sqrt{{}_2Y_0^* / {}_2V_0^*}. \quad (39)$$

3.3 Time-varying function of energy ratio

The rate at which energy is supplied to the SDOF system by ground acceleration $a_g(t)$ is defined as

$$e_I(t) = \dot{E}_I(t) / m = -a_g(t) \dot{y}(t), \quad (40)$$

$$\text{where } E_I(t)/m = -\int_0^t a_g(t) \dot{y}(t) dt. \quad (41)$$

In Eq. (41), $E_I(t)/m$ is the cumulative energy input per unit mass in the range $[0, t]$, and m is the mass of the SDOF system. Ohi et al.²¹⁾ proposed *energy rate spectra* for linear SDOF systems with viscous damping. The *energy rate* defined by Eq. (40) is identical to these *energy rate spectra*. Thus, $e_I(t)$ is denoted as the *energy ratio* for simplicity. Substituting Eqs. (1) and (27) into Eq. (40), $e_I(t)$ can be rewritten as

$$e_I(t) = -a_g(t) \dot{y}(t) = \left\{ \sum_{n=-N}^N c_n \exp(i\omega_n t) \right\} \left\{ \sum_{n=-N}^N c_n H_{CVV}(i\omega_n) \exp(i\omega_n t) \right\}. \quad (42)$$

Similarly, the rate at which energy is supplied to the SDOF system by ground acceleration $a_g^*(t)$ is expressed as

$$e_I^*(t) = -a_g^*(t) \dot{y}^*(t) = \left\{ \sum_{n=-N}^N c_n \operatorname{sgn}(\omega_n) \exp(i\omega_n t) \right\} \left\{ \sum_{n=1}^N c_n \operatorname{sgn}(\omega_n) H_{CVV}(i\omega_n) \exp(i\omega_n t) \right\}. \quad (43)$$

The time-varying function of the energy ratio, $\widehat{e}_I(t)$, is defined as

$$\widehat{e}_I(t) = \{e_I(t) + e_I^*(t)\}/2. \quad (44)$$

Substituting Eqs. (42) and (43) into Eq. (44), $\widehat{e}_I(t)$ can be written as the Fourier series

$$\widehat{e}_I(t) = \sum_{n=-N+1}^{N-1} E_n^* \exp(i\omega_n t), \quad (45)$$

$$\text{where } E_n^* = \begin{cases} \sum_{n_1=n+1}^N \{H_{CVV}(i\omega_{n_1}) + H_{CVV}(-i\omega_{n_1-n})\} c_{n_1} c_{-(n_1-n)} & : n \geq 0 \\ E_{-n}^* & : n < 0 \end{cases}. \quad (46)$$

Equations (45) and (46) are derived in Appendix B. The integral of Eq. (45) from $[0, t_d]$ is

$$\int_0^{t_d} \widehat{e}_I(t) dt = \int_0^{t_d} \sum_{n=-N+1}^{N-1} E_n^* \exp(i\omega_n t) dt = t_d E_0^* = 2t_d \sum_{n_1=1}^N \operatorname{Re}\{H_{CVV}(i\omega_{n_1})\} |c_{n_1}|^2. \quad (47)$$

Equation (47) is identical to the total input energy per unit mass derived by Ordaz et al.⁷⁾. Therefore, the time-varying function of the cumulative energy input per unit mass $\widehat{E}_I(t)/m$ is defined as

$$\widehat{E}_I(t)/m = \int_0^t \widehat{e}_I(t) dt = \int_0^t \sum_{n=-N+1}^{N-1} E_n^* \exp(i\omega_n t) dt \approx E_I(t)/m. \quad (48)$$

In the following discussion, the time-varying function $\widehat{E}_I(t)/m$ is considered as an approximation

of the cumulative energy input per unit mass in the range $[0, t]$.

3.4 Time-varying function of momentary input energy

Following Inoue and his coauthors^{3), 4)}, the momentary input energy per unit mass is defined as

$$\Delta E(t)/m = - \int_t^{t+\Delta t} a_g(t) \dot{y}(t) dt. \quad (49)$$

In Eq. (49), Δt is the duration of a half-cycle of the structural response. Equation (49) can then be rewritten using Eq. (48). Using Eq. (45), the average of the momentary input energy ratio per unit mass, $(1/\Delta t)(\Delta E/m)$, is approximated as

$$\frac{1}{\Delta t} \frac{\Delta E(t)}{m} = - \frac{1}{\Delta t} \int_t^{t+\Delta t} a_g(t) \dot{y}(t) dt \approx \frac{1}{\Delta t} \int_{t-\Delta t/2}^{t+\Delta t/2} \widehat{e}_l(t) dt = \frac{1}{\Delta t} \int_{t-\Delta t/2}^{t+\Delta t/2} \sum_{n=-N+1}^{N-1} E_n^* \exp(i\omega_n t) dt. \quad (50)$$

Note that in Eq. (50), the range of integration changes from $[t, t + \Delta t]$ to $[t - \Delta t/2, t + \Delta t/2]$. This is because the average of the momentary input energy ratio at time t is defined as the average of \widehat{e}_l in the range $[t - \Delta t/2, t + \Delta t/2]$. The calculation of Eq. (50) assumes that Δt can be approximated as half of the response period T' defined in Eq. (39). By calculating the integral in Eq. (50), the time-varying function of the momentary input energy per unit mass can be rewritten as

$$\frac{1}{\Delta t} \frac{\widehat{\Delta E}(t)}{m} = \sum_{n=-N+1}^{N-1} E_{\Delta n}^* \exp(i\omega_n t) \approx \frac{1}{\Delta t} \frac{\Delta E(t)}{m}, \quad (51)$$

$$\text{where } E_{\Delta,0}^* = E_0^*, E_{\Delta,n}^* = \frac{\sin(\omega_n \Delta t/2)}{\omega_n \Delta t/2} \cdot E_n^*, E_{\Delta,-n}^* = \overline{E_{\Delta,n}^*}. \quad (52)$$

The time-varying momentary input energy can be calculated from the Fourier amplitude and phase difference of the ground acceleration, and the properties of the linear SDOF system. Thus, it remains unchanged if the phase angle in all harmonics of the ground acceleration is shifted by a constant.

4. NUMERICAL EXAMPLES

4.1 Ground motion data

This study uses the horizontal major component of the Osaka Gas Fukiai record (FKI) from the 1995 Hyogo-ken Nanbu Earthquake and the horizontal major component from Sendai Government Office building #2 (SND) recorded during the 2011 earthquake that affected the Pacific coast of Tohoku²²⁾. Twelve semi-artificial ground accelerations are generated for each record by shifting the phase angle according to Eq. (21). In this article, the constant phase angle shift for all harmonics, $\Delta\phi_0$, ranges from $0-11\pi/12$ in steps of $\pi/12$; the FKI and SND data are generated for each record. The time interval of each ground acceleration is 0.01 s. The data length of each record, after adding 0's for fast Fourier transform (FFT) analysis, is 81.92 s for FKI and 327.68 s for SND.

4.2 Envelope function of ground acceleration

First, the envelope function of ground acceleration $\alpha(t)$ is calculated and compared to the ground acceleration $a_g(\Delta\phi_0, t)$. Figure 2(a) compares $a_g(\Delta\phi_0, t)$ and $\alpha(t)$ for FKI, and Fig. 2(b) shows the time-history of the ratio $a_g(\Delta\phi_0, t)/\alpha(t)$. For SND, $a_g(\Delta\phi_0, t)$ and $\alpha(t)$, and the time-history of the ratio $a_g(\Delta\phi_0, t)/\alpha(t)$, are shown in Fig. 3.

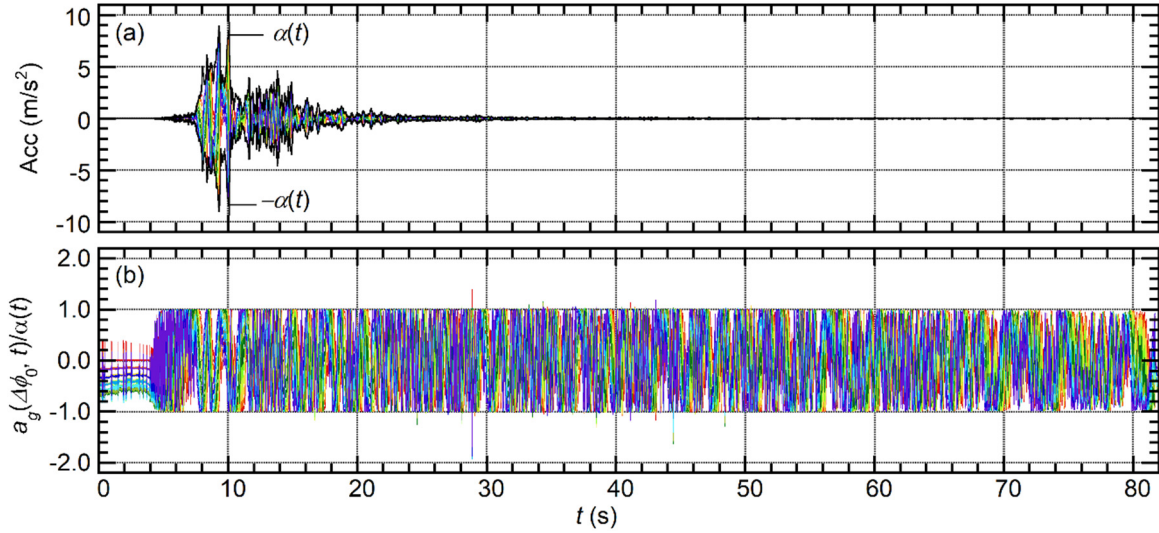


Fig. 2 Validation of the envelope function of ground acceleration (FKI)

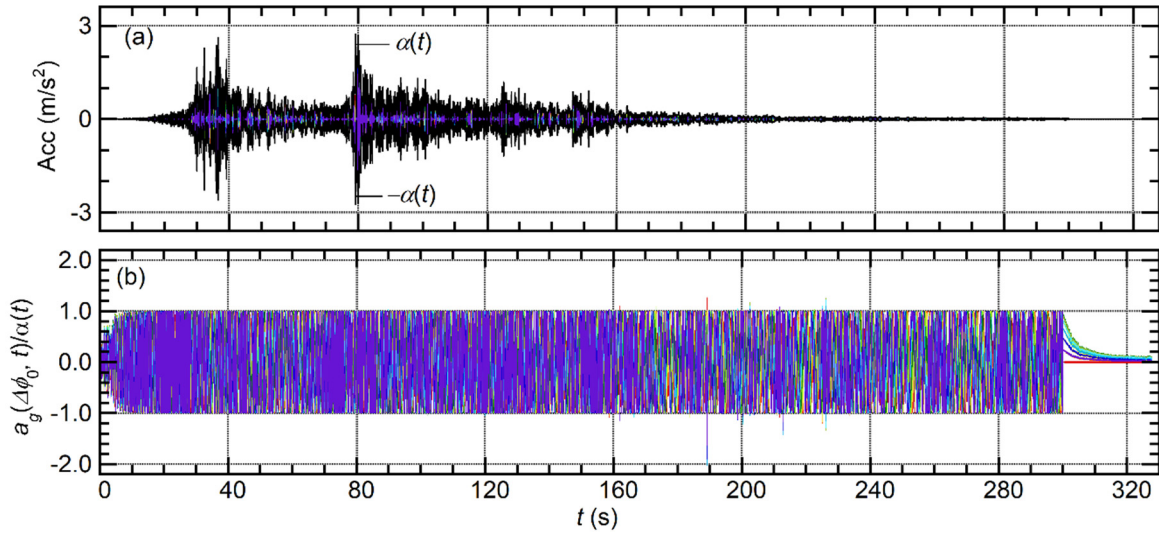


Fig. 3 Validation of the envelope function of ground acceleration (SND)

Figure 2(a) confirms that the whole FKI waveform is unaffected by shifting the phase angle. In addition, the ratio $a_g(\Delta\phi_0, t)/\alpha(t)$ varies within the range $[-1, 1]$, except in limited cases, as shown in Fig. 2(b). Note that the point at which the absolute value of $a_g(\Delta\phi_0, t)/\alpha(t)$ exceeds 1 is in the range where the envelope function is very small ($t > 24$ s); this is actually a numerical artifact. Similar

observations can be made for the SND group. In Fig. 3(b), the absolute value of $a_g(\Delta\phi_0, t)/\alpha(t)$ becomes drastically smaller when $t > 300$ s, corresponding to the part where 0's were added for the FFT.

From Figs. 2(b) and 3(b), the maximum of $|a_g(\Delta\phi_0, t)/\alpha(t)|$ is close to 1.0, except for (i) the first 5 s and (ii) the part where 0's were added for FFT analysis. Therefore, the envelope function shown in Eq. (13) fits well to the acceleration $a_g(\Delta\phi_0, t)$.

Next, discussion focuses on the difference between the time-histories of ground acceleration after shifting the phase angle. Figure 4 shows the time-history of each ground motion group over a 2-s period. The time-histories differ locally according to the value of $\Delta\phi_0$. In addition, all ground accelerations are enveloped by $\alpha(t)$.

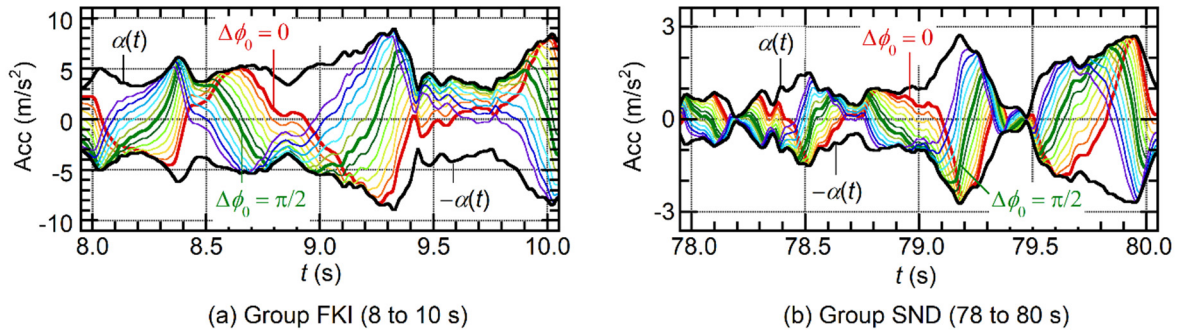


Fig. 4 Difference in the time-history of acceleration caused by phase shift

4.3 Validation of the time-varying function of energy input to a linear SDOF model

4.3.1 Model parameters

The following subsections analyze the time-history of the linear SDOF model using the shifted ground acceleration $a_g(\Delta\phi_0, t)$. Previous studies^{13)–17)} have shown that the following two points are important in obtaining better predictions of the nonlinear response of the structure: (i) the maximum momentary input energy and (ii) the cumulative input energy until the maximum momentary energy input. Therefore, it should be possible to validate the time-varying functions given by Eqs. (48) and (51).

The mass of the SDOF system m is assumed to be 1.0 t. The natural period of the SDOF model T is set to be either 1.0 s or 4.0 s to simulate the response of traditional earthquake-resistant building structures and base-isolated structures, respectively. The viscous damping ratio h is set to 0.10 following a study by Akiyama^{1), 2)}, and the complex damping ratio β is set to 0. The Newmark-Beta method is applied for the numerical integration. The time interval for integration is set to 0.005 s. The number of time-history analyses is $2 \times 2 \times 12 = 48$ cases.

4.3.2 Cumulative energy input per unit mass

Figures 5–8 compare the time-histories of the cumulative energy input obtained from time-history analysis and the time-varying function in Eq. (48). From Fig. 5(a), the time-varying function consistently agrees with the time-history analysis results for the FKI group and $T = 1.0$ s. In addition, Eq. (48) tends to give the median value of the twelve time-history analysis results, as shown in Fig. 5(b). Similar observations can be found for the SND group and $T = 1.0$ s (Fig. 6), as well as for $T = 4.0$ s (Figs. 7, 8). Therefore, the time-history of the cumulative energy input per unit mass can be approximated by Eq. (48). A comparison of Figs. 5 and 7 suggests that the difference in time-histories caused by the phase shift is more significant for $T = 4.0$ s (Fig. 7) than for $T = 1.0$ s (Fig. 5). However, as shown in Fig. 7(a), the difference caused by the phase shift is limited.

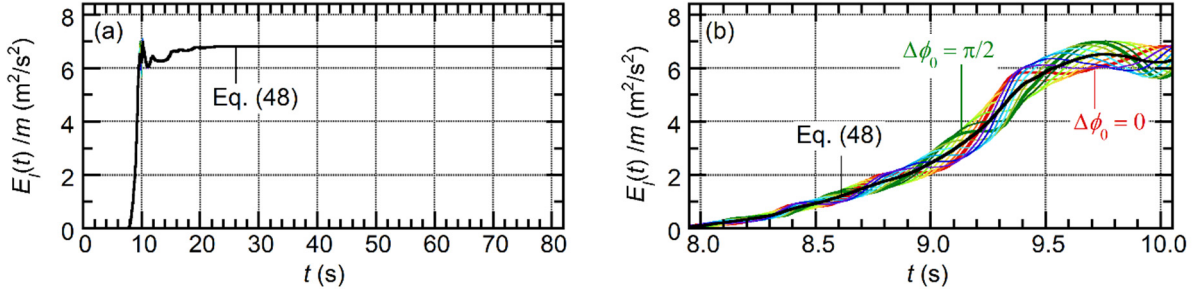


Fig. 5 Time-histories of cumulative energy input (FKI, $T = 1.0$ s)

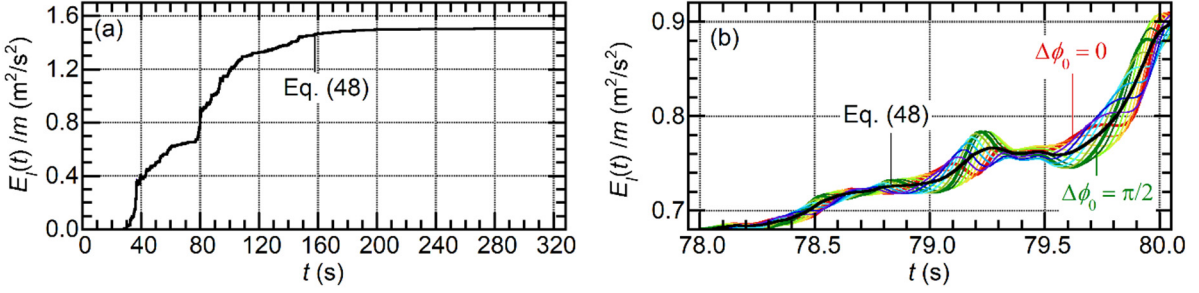


Fig. 6 Time-histories of cumulative energy input (SND, $T = 1.0$ s)

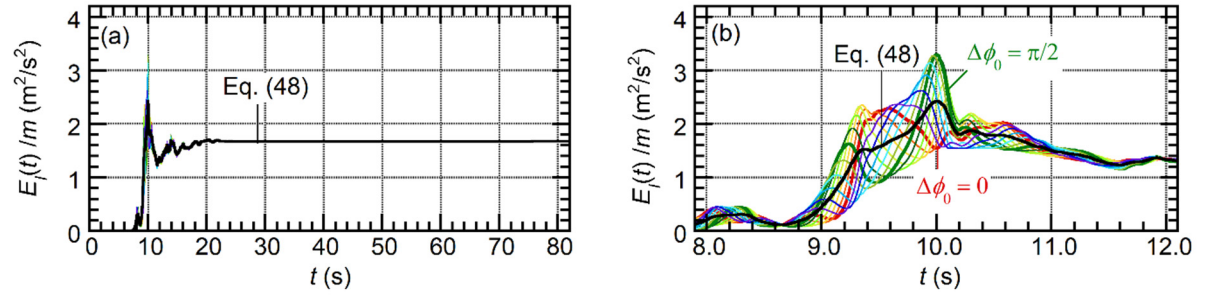


Fig. 7 Time-histories of cumulative energy input (FKI, $T = 4.0$ s)

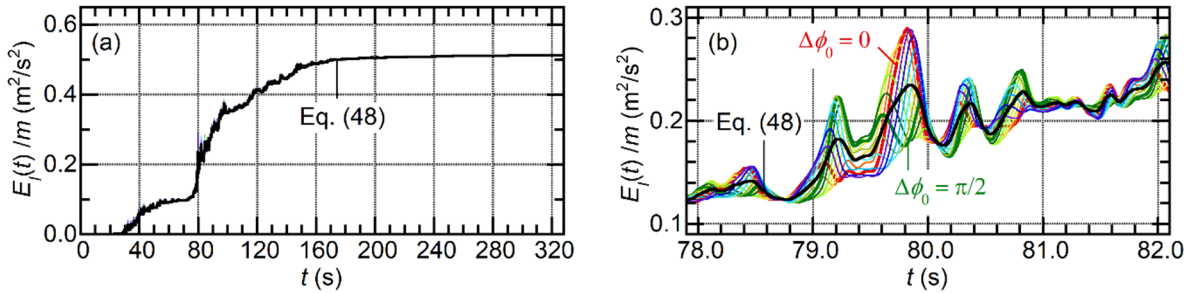


Fig. 8 Time-histories of cumulative energy input (SND, $T = 4.0$ s)

4.3.3 Momentary energy input per unit mass

Next, the time-varying function of the momentary input energy (Eq. (51)) is validated. Figure 9 shows the averaged time-history of the momentary input energy. For $T = 1.0$ s, the time-history of the momentary input energy ratio per unit mass, $(1/\Delta t)(\Delta E/m)$, is smoothed by considering the averaged time-history analysis results, as shown in Fig. 9(a). In contrast, the averaged time-history analysis results are not smooth for $T = 4.0$ s, as shown in Fig. 9(b).

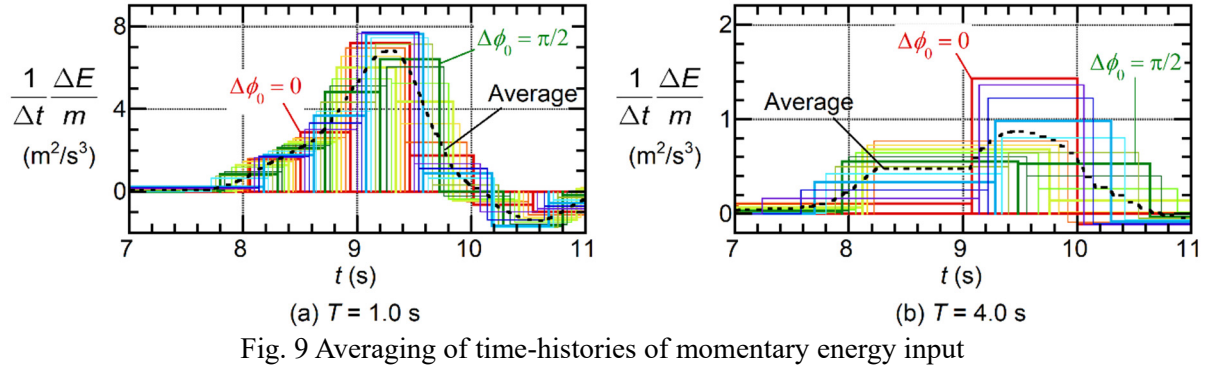


Figure 10 compares the averaged time-history analysis (shown in Fig. 9) and the time-varying function of the momentary input energy (Eq. (51)). The time-varying function agrees well for $T = 1.0$ s, but for $T = 4.0$ s, there are conspicuous differences. In particular, the variation in shorter periods of the time-varying function is noticeable in the SND group, as shown in Fig. 10(b). Comparisons of the coefficients in Eq. (51) are presented in Appendix C.

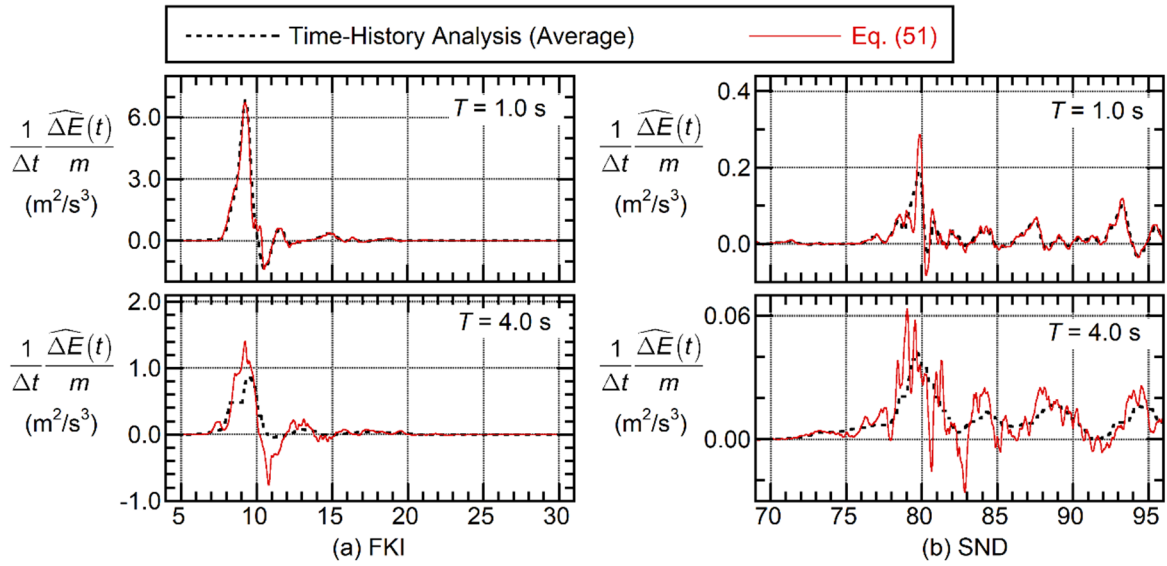


Fig. 10 Comparison of the time-histories of the momentary energy input

To understand why the compatibility of the time-varying function depends on the natural period of the system, Fig. 11 compares the assumed duration of a half-cycle of the structural response Δt using Eq. (51) with that obtained from the time-history analysis. Here, $\Delta t = T'/2$ is assumed from the response period defined in Eq. (39), which is used to calculate Eq. (51), while the value obtained from time-history analysis is taken as the half-cycle of the maximum momentary energy input.

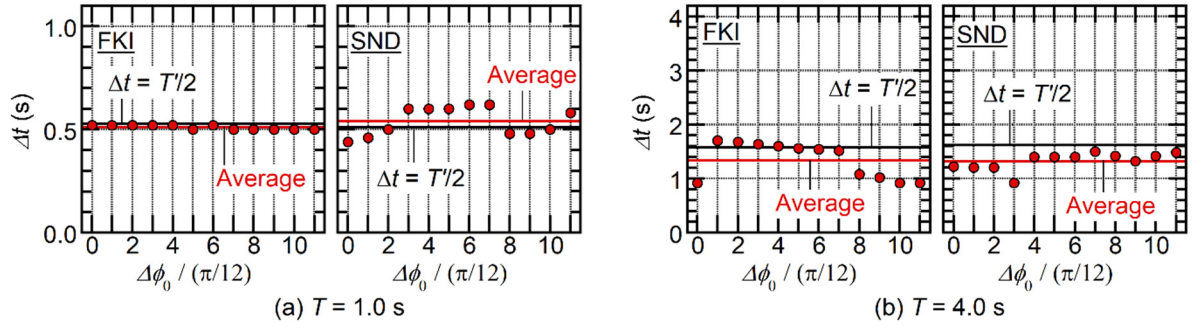


Fig. 11 Comparison of the duration of a half-cycle of the structural response

As shown in Fig. 11(a), $\Delta t = T'/2$ approximates the averaged time-history analysis results for $T = 1.0$ s, especially for FKI, where the variation in the time-history analysis results is very small. In contrast, for $T = 4.0$ s, the difference between $\Delta t = T'/2$ and the averaged time-history analysis results is noticeable, as shown in Fig. 11(b). The variation in the time-history analysis results is larger for the FKI group. One reason why the results from Eq. (51) differ noticeably from the time-history analysis results for $T = 4.0$ s is that the value of Δt used in Eq. (51) is appreciably different from the time-history analysis results.

As stated earlier, one of the target engineering parameters is the maximum momentary input energy per unit mass, $\Delta E_{\max}/m$. This can be calculated as the maximum value of $\Delta E(t)/m$ defined in Eq. (49). Here, $\Delta E(t)/m$ is estimated as

$$\frac{\Delta E(t)}{m} \approx \int_{t-\Delta t/2}^{t+\Delta t/2} \frac{1}{\Delta t} \frac{\widehat{\Delta E}(t)}{m} dt = \int_{t-\Delta t/2}^{t+\Delta t/2} \sum_{n=-N+1}^{N-1} E_{\Delta n}^* \exp(i\omega_n t) dt. \quad (53)$$

The maximum momentary input energy per unit mass, $\Delta E_{\max}/m$, is evaluated as the maximum value of $\Delta E(t)/m$ (Eq. (53)) in the range $[0, t_d]$. For convenience, the equivalent velocity of the maximum momentary input energy is defined as

$$V_{\Delta E} = \sqrt{2\Delta E_{\max}/m}. \quad (54)$$

Figure 12 compares the equivalent velocity $V_{\Delta E}$ predicted from the time-varying function and the time-history analysis results. As shown in Fig. 12(a), the predicted $V_{\Delta E}$ agrees well with the time-history analysis results for $T = 1.0$ s. In addition, the predicted $V_{\Delta E}$ slightly overestimates the time-history analysis results for $T = 4.0$ s in the case of the FKI group, whereas the predicted $V_{\Delta E}$ is close to the time-history analysis results for the SND group.

The overestimation for $T = 4.0$ s with the FKI data occurs because, as shown in Fig. 10(a), the value calculated from Eq. (51) is larger than the averaged time-history from $t = 8-10$ s, when the peak of the time-varying function occurs. In contrast, with the SND data, the variation in the shorter period of the time-varying function is cancelled by the integration in Eq. (53) for $T = 4.0$ s. This is why the predicted $V_{\Delta E}$ is close to the time-history analysis results in this case.

As discussed in previous studies^{1)-5), 11)}, the total input energy E_I and the maximum momentary input energy ΔE_{\max} to the nonlinear SDOF system can be predicted using the *effective period*, which considers the elongation of the natural period as a result of nonlinearities. Considering (i) the accuracy of the effective period and (ii) the unavoidable scattering of the nonlinear peak response caused by local differences in the ground acceleration, the accuracy of the predicted $V_{\Delta E}$ is acceptable for this purpose.

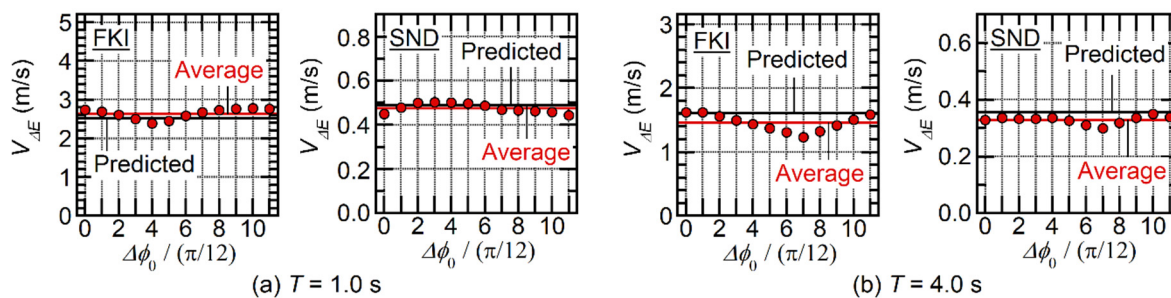


Fig. 12 Accuracy of the predicted equivalent velocity of the maximum momentary input energy

5. CONCLUSIONS

In this article, a time-varying function of the momentary energy input to a linear SDOF system has been formulated. The main conclusions and results of this article are as follows.

1. The time-varying function of the ground acceleration is similar to the envelope of ground acceleration. In addition, the time-varying function can be calculated from the Fourier amplitude and the phase difference of all harmonics. Therefore, it remains unchanged if the phase angle in all harmonics of the ground acceleration is shifted by a constant.
2. The time-varying functions of the displacement and velocity responses, as well as the cumulative and momentary energy inputs of the linear SDOF system, are formulated in the form of Fourier series. They can be calculated from the properties of the linear SDOF system and the Fourier amplitude and phase difference of all harmonics. Those functions are independent of the unavoidable “fluctuations” caused by local differences in the ground acceleration.
3. The time-varying function of the cumulative energy input of the linear SDOF system agrees well with the time-history analysis results. Therefore, the time-varying function of the cumulative energy input formulated in this article provides a good approximation for evaluating the time-history of the cumulative energy input.
4. The time-varying function of the momentary energy input of the linear SDOF system agrees well with the time-history analysis results. The predicted equivalent velocity of the maximum momentary input energy agrees well with the time-history analysis results.

From conclusions 3 and 4, the peak displacement and the cumulative energy of the nonlinear structure can be predicted by using the time-varying functions formulated in this article. The next phase of this study should consider: (a) predictions of the momentary input energy spectrum for linear and nonlinear SDOF systems, and (b) predictions of the cumulative viscous damping energy and hysteresis energy of nonlinear structures using viscous and complex damping.

ACKNOWLEDGMENT

The ground motions records used in this article were originally offered by Osaka Gas Co., Ltd., and BRI Strong Motion Observation. We thank Stuart Jenkinson, PhD, from Edanz Group (<https://en-author-services.edanzgroup.com/>) for editing a draft of this manuscript.

APPENDIX A: DERIVATION OF TIME-VARYING FUNCTION OF GROUND ACCELERATION

The derivation of Eqs. (11) and (12) from Eq. (10) is shown below. To expand Eq. (10), the parameter n is replaced by n_1 and n_2 as

$$\{\hat{a}_g(t)\}^2 = 2 \left\{ \sum_{n_1=1}^N c_{n_1} \exp(i\omega_{n_1} t) \right\} \left\{ \sum_{n_2=1}^N c_{-n_2} \exp(-i\omega_{n_2} t) \right\}. \quad (\text{A1})$$

Expanding Eq. (A1) and considering that $\omega_{n_1-n_2} = \omega_{n_1} - \omega_{n_2}$, $\{\hat{a}_g(t)\}^2$ can be expressed as

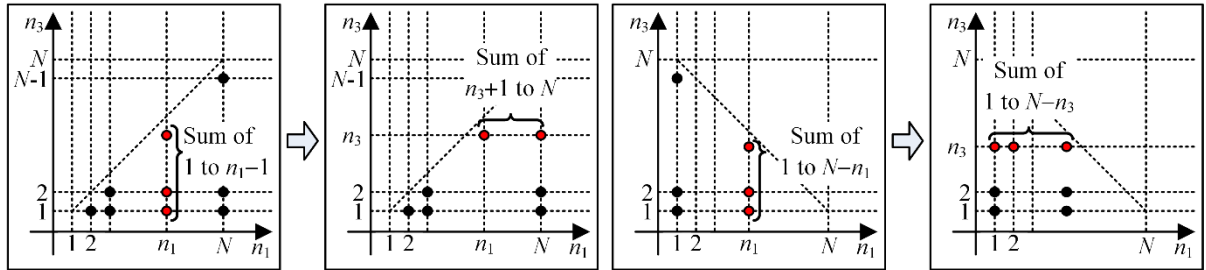
$$\{\hat{a}_g(t)\}^2 = 2 \sum_{n_1=1}^N c_{n_1} c_{-n_1} + 2 \sum_{n_1=2}^N \left\{ \sum_{n_2=1}^{n_1-1} c_{n_1} c_{-n_2} \exp(i\omega_{n_1-n_2} t) \right\} + 2 \sum_{n_1=1}^{N-1} \left\{ \sum_{n_2=n_1+1}^N c_{n_1} c_{-n_2} \exp(-i\omega_{n_2-n_1} t) \right\}. \quad (\text{A2})$$

By setting $n_3 = n_1 - n_2$, the second term of Eq. (A2) can be rewritten as

$$2 \sum_{n_1=2}^N \left\{ \sum_{n_2=1}^{n_1-1} c_{n_1} c_{-n_2} \exp(i\omega_{n_1-n_2} t) \right\} = 2 \sum_{n_1=2}^N \left\{ \sum_{n_3=1}^{n_1-1} c_{n_1} c_{n_3-n_1} \exp(i\omega_{n_3} t) \right\}. \quad (\text{A3})$$

Considering Fig. A1(a) and changing the order of summation, Eq. (A4) can be rewritten as

$$2 \sum_{n_1=2}^N \left\{ \sum_{n_3=1}^{n_1-1} c_{n_1} c_{n_3-n_1} \exp(i\omega_{n_3} t) \right\} = 2 \sum_{n_3=1}^{N-1} \left\{ \sum_{n_1=n_3+1}^N c_{n_1} c_{-(n_1-n_3)} \right\} \exp(i\omega_{n_3} t). \quad (\text{A4})$$



(a) Eq. (A3) (Second term of Eq. (A2))

(b) Eq. (A5) (Third term of Eq. (A2))

Fig. A1 Calculation of summation in Eqs. (A3) and (A5)

Similarly, by setting $n_3 = n_2 - n_1$, the third term of Eq. (A2) can be rewritten as

$$2 \sum_{n_1=1}^N \left\{ \sum_{n_2=n_1+1}^N c_{n_1} c_{-n_2} \exp(-i\omega_{n_2-n_1} t) \right\} = 2 \sum_{n_1=1}^{N-1} \left\{ \sum_{n_3=1}^{N-n_1} c_{n_1} c_{-(n_1+n_3)} \exp(-i\omega_{n_3} t) \right\}. \quad (\text{A5})$$

Considering Fig. A1(b) and changing the order of summation, Eq. (A5) can be rewritten as

$$2 \sum_{n_1=1}^{N-1} \left\{ \sum_{n_3=1}^{N-n_1} c_{n_1} c_{-(n_1+n_3)} \exp(-i\omega_{n_3} t) \right\} = 2 \sum_{n_3=1}^{N-1} \left\{ \sum_{n_1=1}^{N-n_3} c_{n_1} c_{-(n_1+n_3)} \right\} \exp(-i\omega_{n_3} t). \quad (\text{A6})$$

Substituting $n_1 = n_2 - n_3$ into Eq. (A6) gives

$$2 \sum_{n_3=1}^{N-1} \left\{ \sum_{n_1=1}^{N-n_3} c_{n_1} c_{-(n_1+n_3)} \right\} \exp(-i\omega_{n_3} t) = 2 \sum_{n_3=1}^{N-1} \left\{ \sum_{n_2=n_3+1}^N c_{n_2-n_3} c_{-n_2} \right\} \exp(-i\omega_{n_3} t). \quad (\text{A7})$$

Therefore, Eq. (2) can be rewritten as

$$\{\hat{a}_g(t)\}^2 = 2 \sum_{n_1=1}^N c_{n_1} c_{-n_1} + 2 \sum_{n_3=1}^{N-1} \left\{ \sum_{n_1=n_3+1}^N c_{n_1} c_{-(n_1+n_3)} \right\} \exp(i\omega_{n_3} t) + 2 \sum_{n_3=1}^{N-1} \left\{ \sum_{n_2=n_3+1}^N c_{n_2-n_3} c_{-n_2} \right\} \exp(-i\omega_{n_3} t). \quad (\text{A8})$$

Equation (A8) is the expression of the square of the time-varying function of ground acceleration in the form of a Fourier series. By defining each coefficient as in Eq. (12), Eq. (A8) can be written as Eq. (11).

APPENDIX B: DERIVATION OF TIME-VARYING FUNCTION OF ENERGY RATE

The derivation of Eq. (45) is shown below. By substituting Eqs. (42) and (43) into Eq. (44) and replacing the parameter n by n_1 and n_2 , $\hat{e}_I(t)$ can be expressed as

$$\begin{aligned} \hat{e}_I(t) = & \left\{ \sum_{n_1=1}^N c_{n_1} \exp(i\omega_{n_1} t) \right\} \left\{ \sum_{n_2=1}^N H_{CVV}(-i\omega_{n_2}) c_{-n_2} \exp(-i\omega_{n_2} t) \right\} \\ & + \left\{ \sum_{n_1=1}^N H_{CVV}(i\omega_{n_1}) c_{n_1} \exp(i\omega_{n_1} t) \right\} \left\{ \sum_{n_2=1}^N c_{-n_2} \exp(-i\omega_{n_2} t) \right\}. \end{aligned} \quad (\text{A9})$$

The first term of Eq. (A9) can be expanded as

$$\begin{aligned} & \left\{ \sum_{n_1=1}^N c_{n_1} \exp(i\omega_{n_1} t) \right\} \left\{ \sum_{n_2=1}^N H_{CVV}(-i\omega_{n_2}) c_{-n_2} \exp(-i\omega_{n_2} t) \right\} \\ = & \sum_{n_1=1}^N H_{CVV}(-i\omega_{n_1}) c_{n_1} c_{-n_1} + \sum_{n_1=2}^N \left\{ \sum_{n_2=1}^{n_1-1} H_{CVV}(-i\omega_{n_2}) c_{n_1} c_{-n_2} \exp(i\omega_{n_1-n_2} t) \right\}. \quad (\text{A10}) \\ & + \sum_{n_1=1}^{N-1} \left\{ \sum_{n_2=n_1+1}^N H_{CVV}(-i\omega_{n_2}) c_{n_1} c_{-n_2} \exp(-i\omega_{n_2-n_1} t) \right\} \end{aligned}$$

Similarly, the second term of Eq. (A9) can be expanded as

$$\begin{aligned} & \left\{ \sum_{n_1=1}^N H_{CVV}(i\omega_{n_1}) c_{n_1} \exp(i\omega_{n_1} t) \right\} \left\{ \sum_{n_2=1}^N c_{-n_2} \exp(-i\omega_{n_2} t) \right\} \\ = & \sum_{n_1=1}^N H_{CVV}(i\omega_{n_1}) c_{n_1} c_{-n_1} + \sum_{n_1=2}^N \left\{ \sum_{n_2=1}^{n_1-1} H_{CVV}(i\omega_{n_1}) c_{n_1} c_{-n_2} \exp(i\omega_{n_1-n_2} t) \right\}. \quad (\text{A11}) \\ & + \sum_{n_1=1}^{N-1} \left\{ \sum_{n_2=n_1+1}^N H_{CVV}(i\omega_{n_1}) c_{n_1} c_{-n_2} \exp(-i\omega_{n_2-n_1} t) \right\} \end{aligned}$$

Therefore, Eq. (A9) can be rewritten as

$$\begin{aligned} \hat{e}_I(t) = & \sum_{n_1=1}^N \left\{ H_{CVV}(-i\omega_{n_1}) + H_{CVV}(i\omega_{n_1}) \right\} |c_{n_1}|^2 \\ & + \sum_{n_1=2}^N \left[\sum_{n_2=1}^{n_1-1} \left\{ H_{CVV}(i\omega_{n_1}) + H_{CVV}(-i\omega_{n_2}) \right\} c_{n_1} c_{-n_2} \exp(i\omega_{n_1-n_2} t) \right] \\ & + \sum_{n_1=1}^{N-1} \left[\sum_{n_2=n_1+1}^N \left\{ H_{CVV}(i\omega_{n_1}) + H_{CVV}(-i\omega_{n_2}) \right\} c_{n_1} c_{-n_2} \exp(-i\omega_{n_2-n_1} t) \right] \end{aligned} \quad (A12)$$

The second and third terms of Eq. (A12) can be rewritten using a similar method as in Appendix A. Therefore, $\hat{e}_I(t)$ can be expressed in the form of a Fourier series as

$$\begin{aligned} \hat{e}_I(t) = & \sum_{n_1=1}^N \left\{ H_{CVV}(-i\omega_{n_1}) + H_{CVV}(i\omega_{n_1}) \right\} |c_{n_1}|^2 \\ & + \sum_{n_3=1}^{N-1} \left[\sum_{n_1=n_3+1}^N \left\{ H_{CVV}(i\omega_{n_1}) + H_{CVV}(-i\omega_{n_1-n_3}) \right\} c_{n_1} c_{-(n_1-n_3)} \right] \exp(i\omega_{n_3} t) \\ & + \sum_{n_3=1}^{N-1} \left[\sum_{n_2=n_3+1}^N \left\{ H_{CVV}(i\omega_{n_2-n_3}) + H_{CVV}(-i\omega_{n_2}) \right\} c_{n_2-n_3} c_{-n_2} \right] \exp(-i\omega_{n_3} t) \end{aligned} \quad (A13)$$

By defining each coefficient as in Eq. (46), Eq. (A13) can be written as Eq. (45).

APPENDIX C: COMPARISON OF FOURIER COEFFICIENTS OF TIME-VARYING FUNCTION OF MOMENTARY INPUT ENERGY

Figures A2 and A3 show the normalized Fourier coefficient of the time-varying function of momentary input energy, $|E_{\Delta,n}^*|/|E_{\Delta,0}^*|$, as a function of the n^{th} frequency $f_n = \omega_n/(2\pi)$. Here, $2/T'$ ($=1/\Delta t$) is the reciprocal of the assumed duration of a half-cycle of the structural response. As shown in these figures, the normalized coefficient $|E_{\Delta,n}^*|/|E_{\Delta,0}^*|$ decreases rapidly as the frequency f_n increases from 0. In addition, $|E_{\Delta,n}^*|/|E_{\Delta,0}^*|$ becomes very small around $f_n = 2/T', 4/T'$.

For $T = 1.0$ s, $|E_{\Delta,n}^*|/|E_{\Delta,0}^*|$ is less than 0.10 in the range $2/T' < f_n < 4/T'$, and $|E_{\Delta,n}^*|/|E_{\Delta,0}^*|$ is less than 0.01 in the range $4/T' < f_n < 6/T'$, as shown in Fig. A2. For $T = 4.0$ s (Fig. A3), $|E_{\Delta,n}^*|/|E_{\Delta,0}^*|$ is greater than for $T = 1.0$ s, and $|E_{\Delta,n}^*|/|E_{\Delta,0}^*|$ is greater than 0.01 in the range $4/T' < f_n < 6/T'$. This implies that the contribution of the component of $f_n > 2/T'$ in the time-varying function is greater for $T = 4.0$ s than for $T = 1.0$ s. In other words, the contribution of the components in periods shorter than the natural period in Eq. (51) is more significant in the case of $T = 4.0$ s.

In conclusion, the predominant contribution of the shorter-period components in Eq. (51) may be the primary factor in the difference between the time-history analysis results and the time-varying function shown in Fig. 10. Therefore, the compatibility of the time-varying function and the time-history analysis results may depend on the relation between the natural period of the system and the predominant period of the ground acceleration.

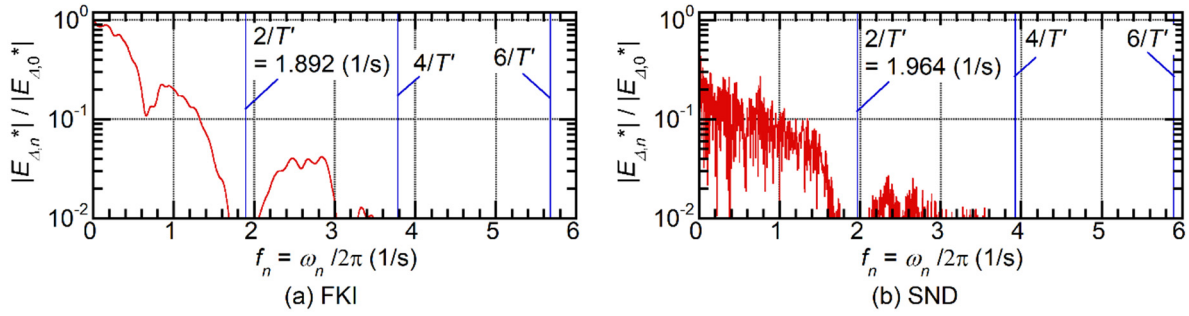


Fig. A2 Normalized Fourier coefficient of time-varying function of momentary input energy ($T = 1.0$ s)

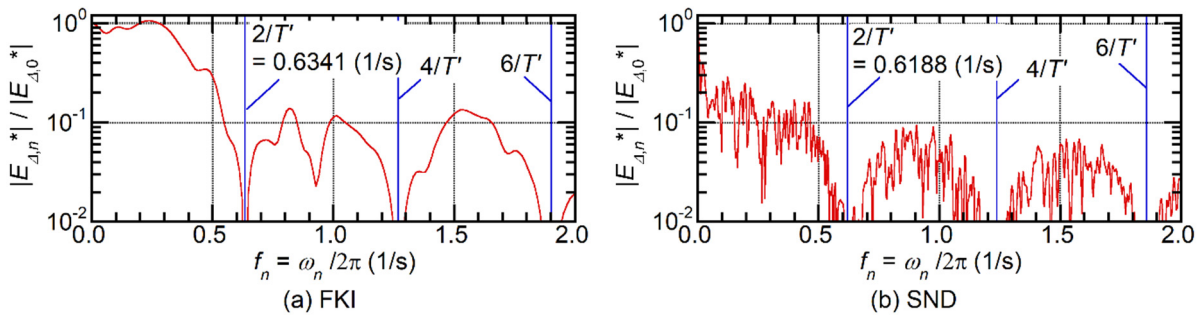


Fig. A3 Normalized Fourier coefficient of time-varying function of momentary input energy ($T = 4.0$ s)

REFERENCES

- 1) Akiyama, H.: *Earthquake-Resistant Limit-State Design for Buildings*, University of Tokyo Press, 321 pp., 1985 (in Japanese).
- 2) Akiyama, H.: *Earthquake-Resistant Design Method for Buildings Based on Energy Balance*, Gihodo Shuppan, 230 pp., 1999 (in Japanese).
- 3) Nakamura, T., Hori, N. and Inoue, N.: Evaluation of Damaging Properties of Ground Motions and Estimation of Maximum Displacement Based on Momentary Input Energy, *Journal of Structural and Construction Engineering*, Architectural Institute of Japan, Vol. 63, No. 513, pp. 65–72, 1998 (in Japanese).
- 4) Hori, N. and Inoue, N.: Damaging Properties of Ground Motions and Prediction of Maximum Response of Structures Based on Momentary Energy Response, *Earthquake Engineering and Structural Dynamics*, Vol. 31, No. 9, pp. 1657–1679, 2002.
- 5) Nakamura, Y. and Kabeyasawa, T.: A Study on Maximum Inelastic Displacement Response Based on Characteristics of Earthquake Motions, *Journal of Structural Engineering*, Architectural Institute of Japan, Vol. 43B, pp. 485–492, 1997 (in Japanese).
- 6) Kuwamura, H., Akiyama, H. and Kirino, Y.: Prediction of Earthquake Energy Input from Smoothed Fourier Amplitude Spectrum, *Journal of Structural and Construction Engineering*, Architectural Institute of Japan, No. 442, pp. 53–60, 1992 (in Japanese).
- 7) Ordaz, M., Huerta, B. and Reinoso, E.: Exact Computation of Input-Energy Spectra from Fourier Amplitude Spectra, *Earthquake Engineering and Structural Dynamics*, Vol. 32, No. 4, pp.597–605, 2003.
- 8) Ohsaki, Y.: On the Significance of Phase Content in Earthquake Ground Motions, *Earthquake Engineering and Structural Dynamics*, Vol. 7, No. 5, pp.427–439, 1979.
- 9) Kuwamura, H.: Limit States and Failure Criteria for Earthquake Resistant Structures, *Journal of Structural and Construction Engineering*, Architectural Institute of Japan, No. 387, pp. 45–54, 1988

- (in Japanese).
- 10) Takahashi, M. and Akiyama, H.: Study on Time History of Energy Input Due to Earthquakes, *Summaries of Technical Papers of Annual Meeting*, Architectural Institute of Japan, Vol. B, pp. 419–420, 1991 (in Japanese) .
 - 11) Fujii, K and Kida, S.: Evaluation of the Maximum Momentary Energy Input to a Structure Considering Phase Characteristics of Ground Motion, *Proceedings of the 16th European Conference on Earthquake Engineering*, 10363, 2018.
 - 12) Izumi, M. and Katsukura, H.: A Fundamental Study on Extraction of Phase-Information in Earthquake Motions, *Journal of Structural and Construction Engineering*, Architectural Institute of Japan, No. 327, pp. 20–28, 1983 (in Japanese).
 - 13) Fujii, K.: Accuracy of Predicted Peak Response of Existing Middle-Rise Steel Reinforced Concrete Building Using Equivalent Linearization Technique, *Journal of Structural and Construction Engineering*, Architectural Institute of Japan, Vol. 81, No. 721, pp. 483–493, 2016 (in Japanese).
 - 14) Fujii, K., Kanno, H. and Nishida, T.: Accuracy of Equivalent Linearization Technique to Predict the Peak Seismic Response of Existing Middle-Rise SRC Building Considering the Phase Characteristics of Record Earthquakes, *Proceedings of the Japan Concrete Institute*, Vol. 38, No. 2, pp. 823–828, 2016 (in Japanese).
 - 15) Fujii, K.: Relationship Between the Maximum Momentary Energy Input and the Peak Displacement of Middle-Rise Existing Steel Reinforced Concrete Building with Brittle Members, *Proceedings of the Japan Concrete Institute*, Vol. 40, No. 2, pp. 745–750, 2018 (in Japanese).
 - 16) Kanno, H., Sakurai, M., Fujii, K. and Nishida, T.: Accuracy of Equivalent Linearization Technique to Predict the Peak Seismic Response of Existing Middle-Rise SRC Building Considering the Phase Characteristics of Record Earthquakes, *Proceedings of the Japan Concrete Institute*, Vol. 37, No. 2, pp. 673–678, 2015 (in Japanese).
 - 17) Kanno, H., Fujii, K., Sakurai, M. and Nishida, T.: Experimental Study on Seismic Energy Response for a Building Model Composed of Shear and Flexural R/C Columns, *Proceedings of the Japan Concrete Institute*, Vol. 38, No. 2, pp. 895–900, 2016 (in Japanese).
 - 18) Kimura, M: On Control of the Characteristics of the Wave in Generating Simulated Earthquake Ground Motions, *Journal of Structural and Construction Engineering*, Architectural Institute of Japan, No. 367, pp. 30–36, 1986 (in Japanese).
 - 19) Fujii, K. and Miyagawa K.: Nonlinear Seismic Response of a Seven-Story Steel Reinforced Concrete Condominium Retrofitted with Low-Yield-Strength-Steel Damper Columns, *Proceedings of the 16th European Conference on Earthquake Engineering*, 10736, 2018.
 - 20) Sagami, Y., Hori, N., Ikago, K. and Inoue, N.: A Study on the Effect of Existence of Frequency Dependency to Damper Force of Base-Isolated Structure, *Journal of Structural and Construction Engineering*, Architectural Institute of Japan, Vol. 77, No. 674, pp. 529–536, 2012 (in Japanese).
 - 21) Ohi, K., Takanashi, K. and Honma, Y.: Energy Input Rate Spectra of Earthquake Ground Motions, *Journal of Structural and Construction Engineering*, Architectural Institute of Japan, No. 420, pp. 1–7, 1991 (in Japanese).
 - 22) Kashima, T., Koyama, S. and Okawa, I.: Strong Motion Records in Buildings from the 2011 off Pacific Coast of Tohoku Earthquake, *Building Research Data*, Building Research Institute, No. 135, 142 pp., 2012 (in Japanese).

(Original Japanese Paper Published: September, 2019)
(English Version Submitted: January 22, 2021)
(English Version Accepted: February 15, 2021)